J. Fluid Mech. (1976), *vol.* 77, *part* 2, *pp.* 209–228
Printed in Great Britain

On the variation and growth of wave-slope spectra in the capillary-gravity range with increasing wind

By STEVEN R. LONG

Center for Marine and Coastal Studies, North Carolina State University, Raleigh†

AND NORDEN E. HUANG

Applied Science Directorate, NASA Wallops Flight Center,
Wallops Island, Virginia 23337

(Received 14 July 1975)

A new laser device has been used to make direct wave-slope measurements in the capillary–gravity range. Owing to the design principles, the digital nature of the system and the use of a laser beam as a probe, the earlier problems of intensity variations and meniscus effects were avoided. Using this new technique, wave-slope spectra both down and across the channel were obtained for different wind conditions, along with corresponding mean-square slope values. Comparisons are made with existing data. The results indicate that a quasi-equilibrium state may exist for each wind speed and that it increases in intensity with increasing wind, which may imply an asymptotic nature for the equilibrium-range coefficient $C_{\alpha\alpha}$. From the data, two significant frictional velocities, 17·5 and 31 cm/s respectively, are identified as critical values for different ranges of wave development.

1. Introduction

The exact relationship between the wind and surface waves is still unknown at the present time. Many theories have been advanced, however, which have been successful to a degree in describing this interaction, such as those of Phillips (1957) and Miles (1957). Much experimental work has also been conducted to verify the theoretical results, but most of the results are in the gravity-wave range. Far less attention has been focused on the higher wavenumber range where the surface-tension force dominates. This is partly due to the fact that only a negligible amount of energy is contained in this range and partly due to the severe limitations on the instrumentation for making measurements.

Since the energy of the waves in the capillary range is no longer measured by the wave height but rather by surface slope, slope measurements are more representative. The asymptotic shape of the slope spectra as proposed by Phillips (1966, p. 118), based on a dimensional analysis, would be

$$S_{\alpha\beta}(n) = C_{\alpha\beta} n^{-1}, \quad n_m \ll n \ll n_\nu, \tag{1}$$

† Present address: NASA Wallops Flight Center, Wallops Island, Virginia 23337.

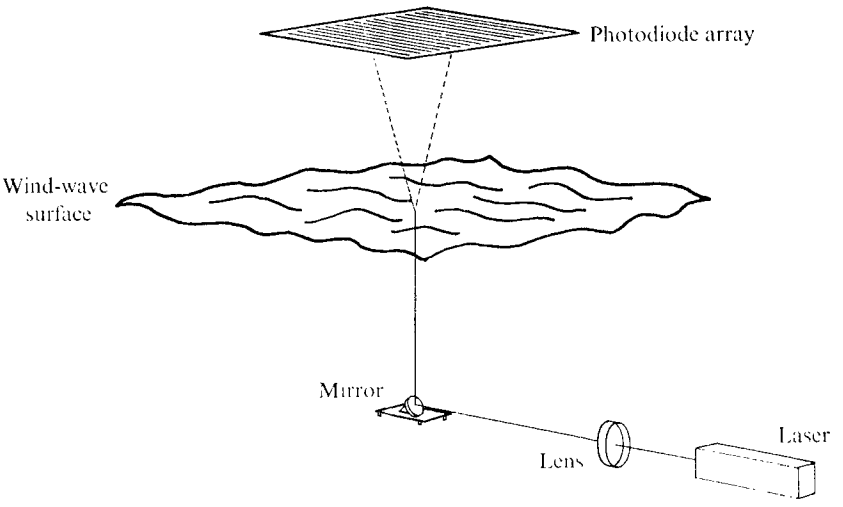

FIGURE 1. The basic operational set-up.

where n_m is the frequency where the phase velocity is a minimum, n_ν is the typical frequency of a viscous wave and the $C_{\alpha\beta}$ are universal constants with α and β equal to 1 or 2, indicating the slope component in the x or y direction respectively. A similar expression in wavenumber space also exists.

A few attempts have been made to measure capillary waves using various methods: the glitter photographs of Cox & Munk (1956), the refractive technique of the laboratory study of Cox (1958) and the reflective method of Wu (1971). However, no definite conclusion could be drawn concerning the existence of the equilibrium range of Phillips other than in the pure gravity range. Recently the interest in the dynamic and statistical properties of capillary waves received a sudden boost because Bragg scattering from capillary–gravity waves caused strong return signals of the microwave radars used in remote sensing techniques such as those reported by Jones *et al.* (1975) and Larson & Wright (1975).

The present study reports the results of laboratory observations made by means of a new device using the refraction of a laser beam to measure the growth of the surface-slope spectrum in the capillary–gravity range. The variation of surface-slope spectra was observed for various fetches and wind conditions.

2. System description

In the present work, the method used by Sturm (1973) to study single one-dimensional trains of capillary waves on currents was developed to produce a device capable of accurate slope measurements, while remaining insensitive to light intensity variations. An array of parallel photodiode strips (each not position sensitive) was employed in this study. Each step in the array responds to the refracted laser beam by generating an output voltage. The photodiode array thus responds to the time variation of the laser beam as it is refracted by wind waves as shown in figure 1. The array may then be positioned to receive

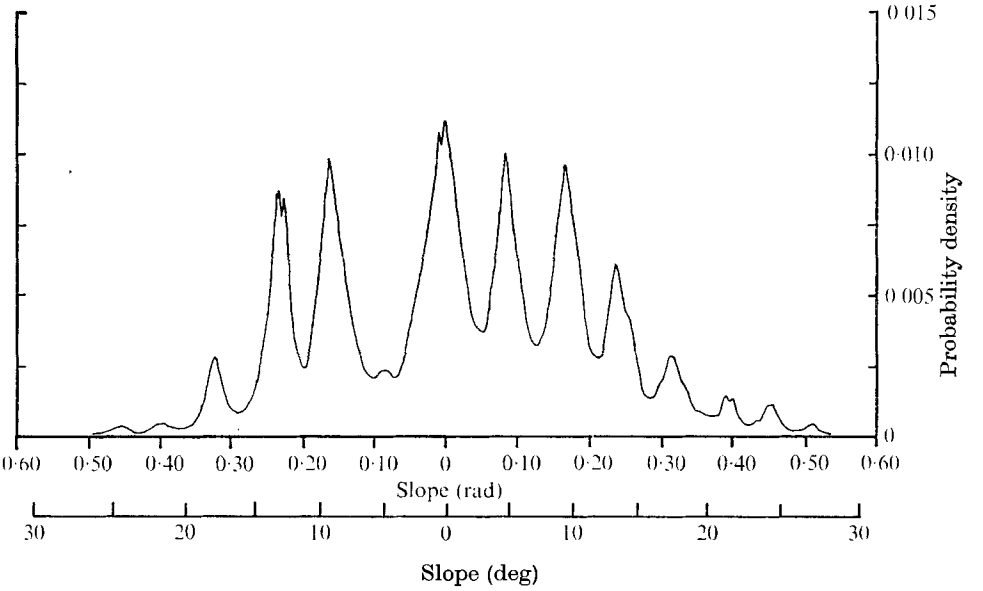

FIGURE 2. The probability density function for a wind speed of 10·4 m/s; down-channel case.

slope information along the wind direction or at any other chosen angle with respect to the wind direction.

To receive the output of the array, a new electronic device was constructed and is described in detail by Huang *et al.* (1974). This device converts the output from the array to binary code. This binary data processor receives the output of the photodiode struck by the laser beam and holds at that value of output while the beam crosses the gap between strips to the next diode. It then locks onto and holds the new value while the process is repeated. The initial output is thus a 'step' approximation of the time record of slope variations. This approximation by steps is then smoothed electronically to give a continuous record of wave-slope variation in time. Thus the limitations of the present device should be considered at the outset. This is more readily done by considering a typical probability density function for the case of the down-channel slope data for a wind speed of 10·4 m/s. This is shown in figure 2. Because the digital device holds one level while the laser spot changes to the next by crossing the gap between the photodiode strips, the resulting change to the next level occurs very fast, so that these digital level changes are not entirely masked by the smoothing process. The probability density in figure 2 reveals this in the gaps between the peaks, indicating a rapid change from one slope level to another, or a low probability of finding the level in the midst of a change. The present device makes use of 18 photodiode elements, 9 on each side of the zero position for no waves. To increase the resolution of the device, one needs only to add more levels, which would result in more peaks being added in figure 2, so that the gaps would disappear as the limit represented by the envelope in figure 2 was approached.

Since the diode strips are equally spaced, and the displacement of the refracted

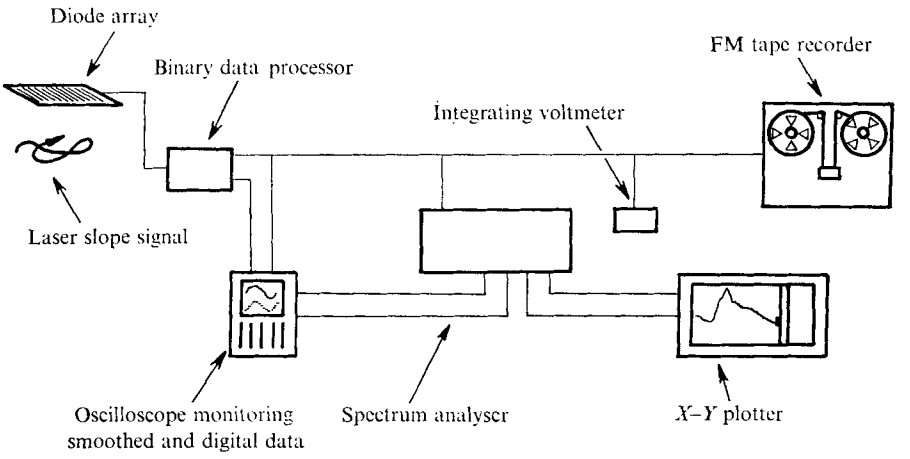

FIGURE 3. The complete system for the present work.

laser spot is nonlinearly related to the surface slope, each spectrum was processed individually by a detailed calibration of known signals generated by the laser and an oscillating mirror. But this calculation to recover the true signal can be avoided easily by a proper spacing of the diodes. The device has also been proved to be sensitive to mechanically and pneumatically generated waves of up to 100 Hz. However there is no independent proof of the absolute accuracy of the measurements. Apparently the limitation is not on the frequency but rather on the spot size at the surface. A detailed discussion of this point will be given later. Both an increase in the number of diodes and the proper spacing are planned for the near future.

The device has a variable reference level so that the effects of room light may be removed, enabling the binary data processor to 'see' only the laser spot. The resulting data for various wind speeds can then be recorded by means of a Hewlett–Packard Model 3960 FM recorder and analysed simultaneously with a Nicolet Model UA-500 spectrum analyser. The complete set-up is shown in figure 3. The wind-wave tank at North Carolina State University was used in this study. This tank is 61 cm by 91 cm in cross-section and 1520 cm long. Because of the presence of a paddle, air intake and beach, the actual maximum usable length for the fetch of the wind waves of the present study is 700 cm. For this study, fetches of 259 cm, 465 cm and 668 cm were used. A tower was used to ensure coverage of the entire array by the laser deflexions, and thus the maximum resolution. The various heights of the array in the tower were used in scaling the resulting slope values. The air flow is generated by a centrifugal-type suction fan, capable of producing 0–20 m/s of wind through the test section. The air flows in through an air intake equipped with fibreglass filters and is measured in the test section by a rotor-type anemometer, a Taylor model 3132 jewelled anemometer 15 cm above the mean water surface. Since the Taylor anemometer measures elapsed feet, each wind-speed measurement was obtained from a time record of elapsed feet over a time period of sufficient length to ensure an accurate reading. The wind-speed values thus represent the mean wind.

Fetch (m)	u_* (cm/s)	Surface tension γ (dynes/cm at 25·0 °C)
4·65	15·8, 18·2, 21·4, 25·0, 29·4	71·57
	32·8, 37·2, 53·0, 70·2	72·00
	82·9, 102	72·00
6·68	15·0, 17·7, 20·8, 24·0	72·00
	27·3, 32·0, 36·5	71·89
	51·5, 67·5, 87·0, 108	72·00
4·65	15·2, 17·8, 20·1, 24·0, 28·5	72·00
	33·0, 36·4, 50·2, 64·5, 83·0	
	108	
2·59	15·5, 18·8, 21·0, 24·7, 28·5	71·79
	33·5, 39·0, 54·0, 68·0, 86·0	
	107	

TABLE 1. Surface-tension values from du Noüy tensiometer measurements

To facilitate comparison with other results, Wu's (1968) expression for the wind velocity distribution is used to obtain an approximate value for the frictional velocity. This expression is just

$$u_c/u_* = 5{\cdot}75 \log (yg/u_*^2) + 11{\cdot}2, \tag{2}$$

where u_c is the wind velocity measured at a height y above the mean surface and corrected by subtracting the phase velocity of the waves with a frequency at the peak of the spectrum, and g is the gravitational acceleration. Granted that different tanks may have different turbulence structures, this expression represents a good mean of the results of the different laboratory studies discussed in Wu (1968). This will give a meaningful u_* for a comparison with other studies.

Before each run, water was sampled from the beach area under steady-state wind conditions and the surface tension measured by means of a Cenco model 70530 du Noüy tensiometer. The samples thus represented the worst case, since they were taken from the area into which the wind would push any surface film. The results are shown in table 1.

3. Data taking

A 7 min record was made for each case. Recording was delayed for several minutes at each new wind setting to ensure steady-state conditions. Both down- and cross-channel slope spectra were obtained for various wind speeds ranging from 3·28 to 12·7 m/s. Two special cases were also investigated: the spectra of the front and back slopes, respectively, of the waves at a wind speed of 3·6 m/s. This was done by positioning the array such that the zero spot for no waves was at one end of the array, resulting in the laser 'looking' exclusively at either the front or the back slopes of the waves, with respect to their direction of travel. The 7 min data sets were analysed simultaneously as they were recorded by

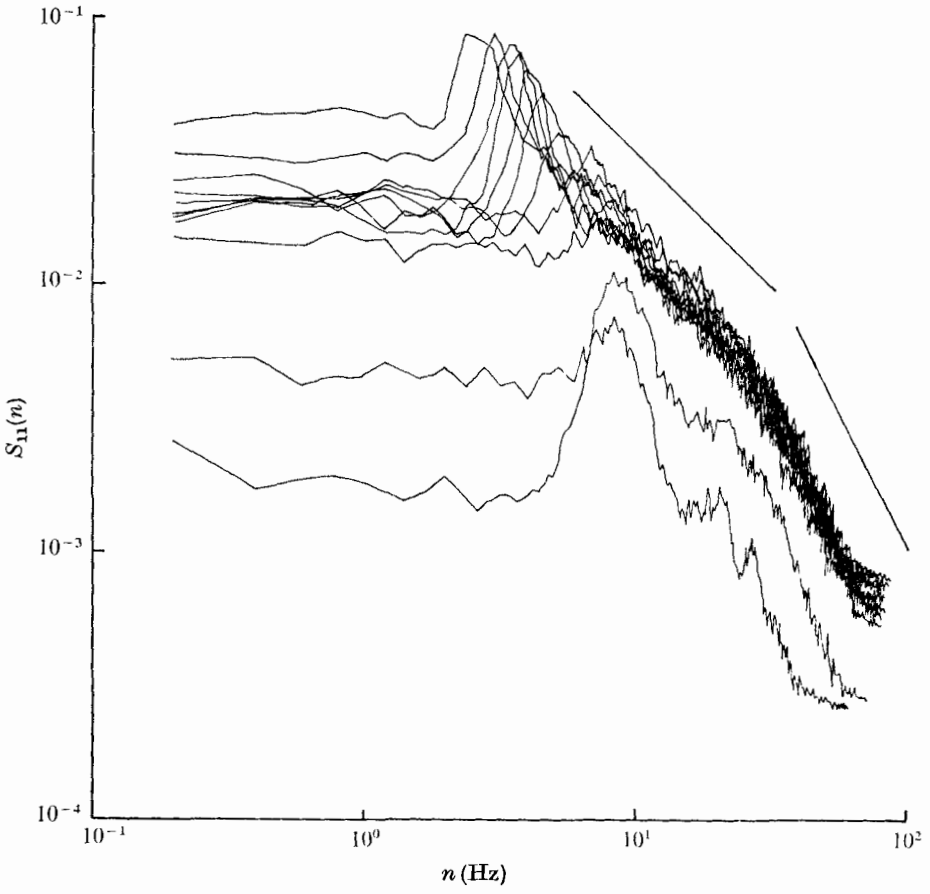

FIGURE 4. The growth of the wind wave spectrum. Fetch constant at 259 cm, wind increasing from 3·36 m/s ($u_* = 15{\cdot}5$ cm/s) to 12·5 m/s ($u_* = 107$ cm/s).

means of a Nicolet model UA-500 spectrum analyser operating over a frequency range from zero to 100 Hz, and using 320 s of the data to produce an average of 64 spectra, with 128 degrees of freedom. The r.m.s. surface slopes were measured by a Disa type 55D35 r.m.s. (integrating) voltmeter. A Hewlett–Packard model 7004B X–Y recorder was then used to produce the frequency spectrum of the slope on a full logarithmic scale. Also, a Nicolet model UC-202C correlator was used to produce the probability density, cumulative distribution and autocorrelation of the different data records.

4. Results

In order to facilitate the discussion, the results are divided into several categories.

The general shape of the spectra

The data collected in the present study support the idea of an eventual equilibrium range in capillary–gravity waves in general, but differ in specific detail

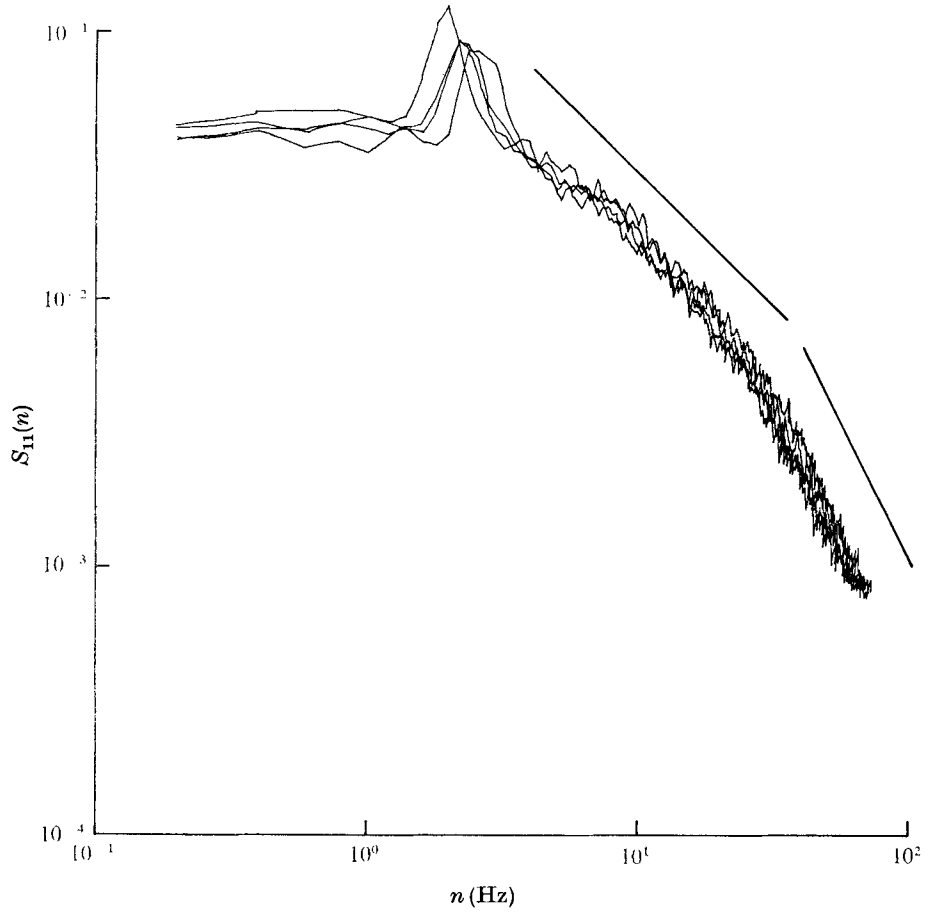

FIGURE 5. The effect of fetch with constant wind. Wind constant at 12·5 m/s ($u_* = 105$ cm/s), fetch values 259 cm, 465 cm (2 spectra) and 668 cm.

from the formula suggested by Phillips (1966). The general shape of the down-channel slope spectrum can be seen from figure 4, where eleven spectra measured at a fetch of 259 cm with a wind speed of from 3·36 m/s ($u_* = 15{\cdot}5$ cm/s) to 12·5 m/s ($u_* = 107$ cm/s) are presented. Except at extremely low wind speeds ($u_* < 20$ cm/s), the spectra tend to crowd together with a low rate of increase in magnitude. For frequencies up to 30 Hz, the envelope of the spectra compares favourably with an n^{-1} curve. However, at higher frequencies, the envelope appears to follow an n^{-2} trend. This n^{-2} trend is difficult to explain by a dynamic argument. One possibility is that the steps of the device and their spacing, corresponding to approximately 4° of slope, might miss some of the fine-structure of the signal. This could thus cause a faster decline of the observed spectra in the higher frequency range. The components between 0·2 and 1 Hz are also seen to increase with wind speed, from figure 4. This could not be just an instrument noise level, since that was determined to be far below the observed data, actually off the scale in the figures shown. This implies that it must be data related,

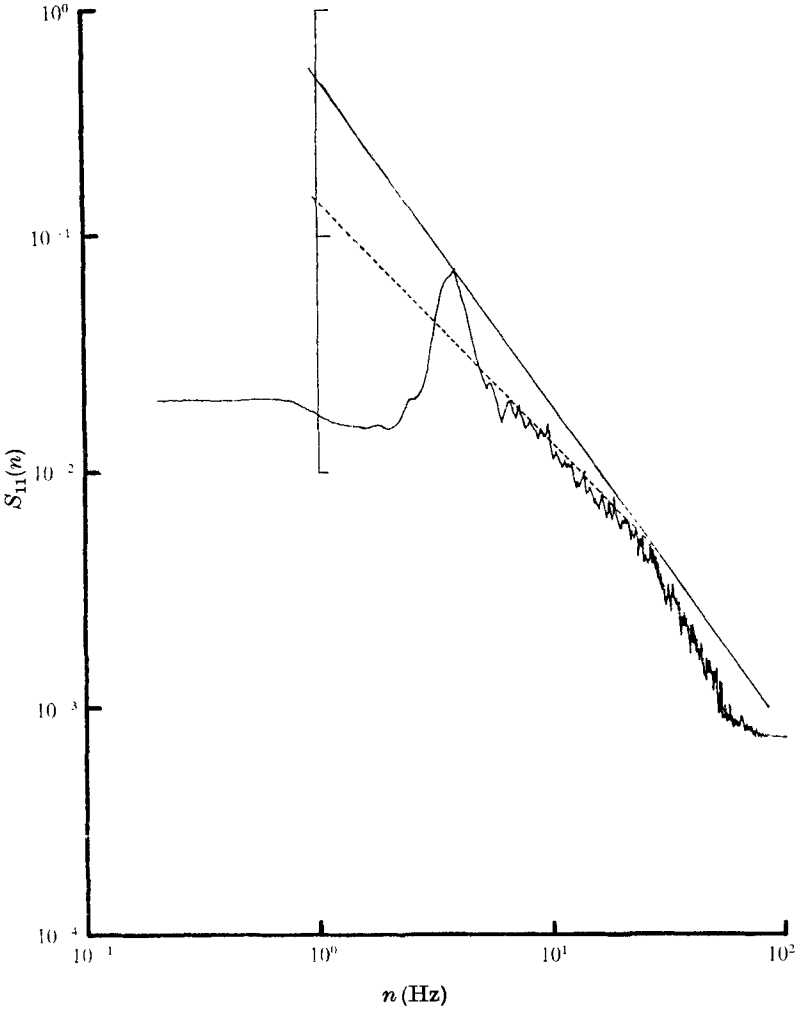

FIGURE 6. The method of measurements of best-fit envelopes shown on the spectrum of down-channel slope values for $u_* = 54$ cm/s and a fetch of 259 cm.

perhaps arising from low-frequency oscillations set up in the tank. Further study may be able to resolve these questions.

In order to show the influence of fetch, four spectra for the same wind speed ($u = 12{\cdot}5$ m/s or $u_* \simeq 105$ cm/s) but different fetches are shown in figure 5. Apart from the location and height of the peak, the higher frequency range again displays a striking similarity, which strongly suggests the existence of an equilibrium range.

To examine the shape of the spectra to get quantitative information, each spectrum was treated individually. From each spectrum, two measurements of best-fit envelopes were made, covering (*a*) the spectrum from the peak up to higher frequencies and (*b*) the spectrum range centred around 13·5 Hz, as shown in figure 6. Then, from each envelope, the slope was read as $1+m$ and the intersection with the vertical axis at $n = 1$ Hz as $S^*_{11}(1)$.

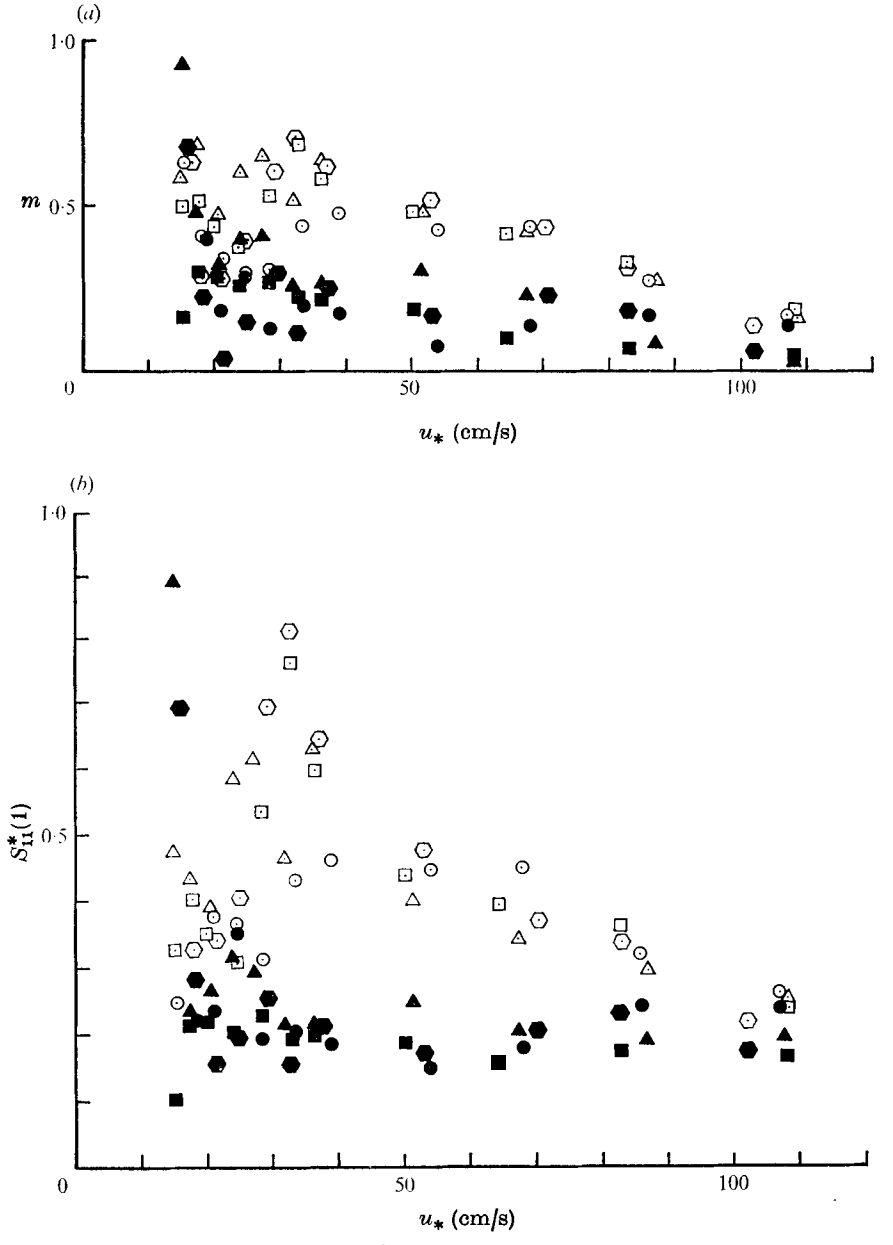

FIGURE 7. (*a*) The slope m and (*b*) $S^*_{11}(1)$ from the best-fit envelopes covering the peak to higher frequency range (open symbols) and from the fit centred on $n = 13{\cdot}5$ Hz (filled symbols). Fetch: ●, 259 cm; ■, ●, 465 cm; ▲, 668 cm.

For the best-fit envelopes, the slope values are given in figure 7 (*a*) and the values of $S^*_{11}(1)$ in figure 7 (*b*). For the envelope covering the peak up to higher frequencies in figure 7 (*a*), the values in general vary rather regularly with u_* after a critical value (~ 30 cm/s) is reached. The trend of the variation is a decrease with increasing u_*. Unfortunately, we do not have data for $u_* > 110$ cm/s, but

the trend strongly suggests the existence of an asymptotic equilibrium range, as proposed by Phillips (1966, p. 118). Since before such an equilibrium is reached the slope of the envelope is still changing, a more general form of the spectrum for the capillary–gravity range is proposed:

$$S_{11}(n) = f(u_*, \gamma, g)/n^{1+m} \tag{3}$$

where $f(u_*, \gamma, g)$ is a dimensional coefficient function for a power-law spectrum dependent on the frictional velocity u_*, surface tension γ and gravitational acceleration g. When $n = 1$,

$$S_{11}(n) = f(u_*, \gamma, g) = S^*_{11}(1). \tag{4}$$

The criterion for choosing these parameters is based on the stability of the capillary–gravity waves. The importance of γ and g has been amply discussed by Phillips (1958, 1966). Since then, Banner & Phillips (1974) and Phillips & Banner (1974) have further suggested the importance of surface drift currents and pre-existing swell for the stability of smaller waves. The surface drift can be related to u_* directly, while the pre-existing swell condition can be parameterized by the location of the peak n_0. However, in the actively wind-generated wave field of the present study, the large-scale waves are also generated by the same wind. In such a wave field, the peak range can be specified again by u_* and the fetch. This seems to call for an additional parameter, the fetch, but the present study did not find any direct evidence of the importance of fetch in the wave range studied. It is, however, possible that in the extreme fetch-limited case, the wave condition at a given location may reach a saturated state which may be designated as a quasi-equilibrium state but not an equilibrium range. Its shape becomes fixed, but not its amplitude. Because of this argument, we are adding only one more parameter, u_*, to the generalized expression (3). By dimensional analysis, (3) can be rewritten as

$$S_{11}(n) = h(\eta) \left(\frac{g^3}{\gamma}\right)^{\frac{1}{4}m(\eta)} \Big/ n^{1+m(\eta)}, \tag{5}$$

where $\eta = (\gamma g)^{\frac{1}{4}}/u_*$. This expression is not unlike the one suggested by Phillips (1966, p. 118):

$$S_{\alpha\beta}(n) = f_{\alpha\beta}(g^3/\gamma n^4)\, n^{-1}. \tag{6}$$

In fact, (5) can be rearranged as

$$S_{11}(n) = F(\eta)\, (g^3/\gamma n^4)^{\frac{1}{4}m(\eta)} n^{-1}. \tag{7}$$

The only difference between (6) and (7) is the additional parameter u_*, and hence the non-dimensional parameter η. Equation (7) may eventually approach (6) at higher u_*. Carrying the extra parameter will make the range of validity of (7), in terms of wind velocity, wider than that of (6). In this overall envelope, the influence of the peak is still noticeable. Since the peak is always changing, the values of m and $S^*_{11}(1)$ can never settle down to any definite value in the range of wind velocity considered here.

If we exclude the influence of the peak by concentrating on the range around $n = 13{\cdot}5$ Hz, the values of m and $S^*_{11}(1)$ then display far less variation, as shown

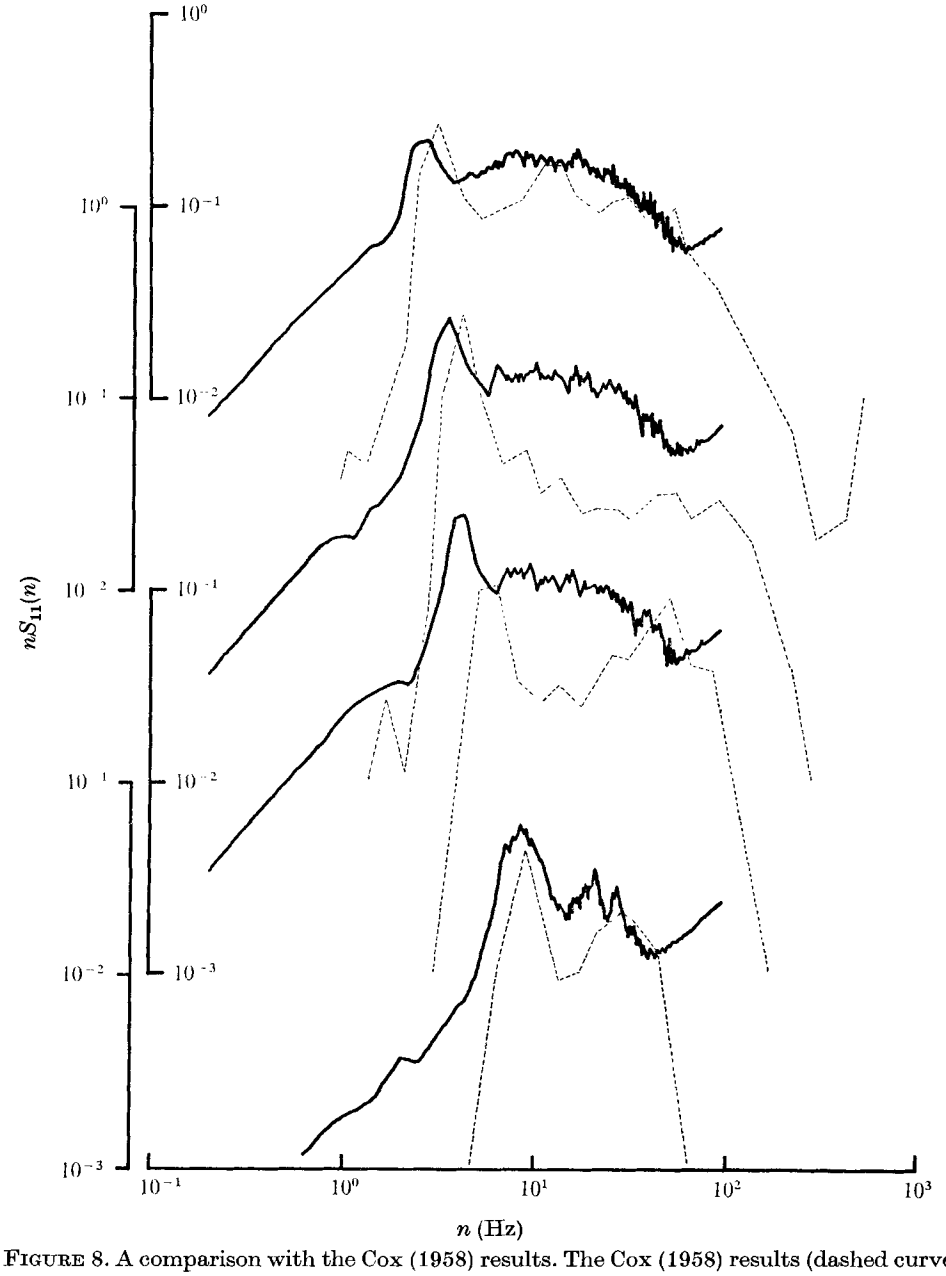

FIGURE 8. A comparison with the Cox (1958) results. The Cox (1958) results (dashed curves) were for wind speeds of 3·18, 6·08, 9·20 and 12·02 m/s at a fetch of 2·14 m. In comparison, the present results (solid curves) are for wind speeds of 3·36, 6·63, 9·53 and 12·5 m/s, at a fetch of 259 cm.

in figures 7 (*a*) and (*b*). Since at 13·5 Hz the energy is equally partitioned between the capillary and gravity forces, (6) and (7) will apply even better. Although the slope m is still changing, $S_{11}^*(1)$ settles down remarkably well to a value around 0·2. This gives a numerical value of the equilibrium-range constant at least an order of magnitude higher than that estimated by Phillips (1966, p. 120).

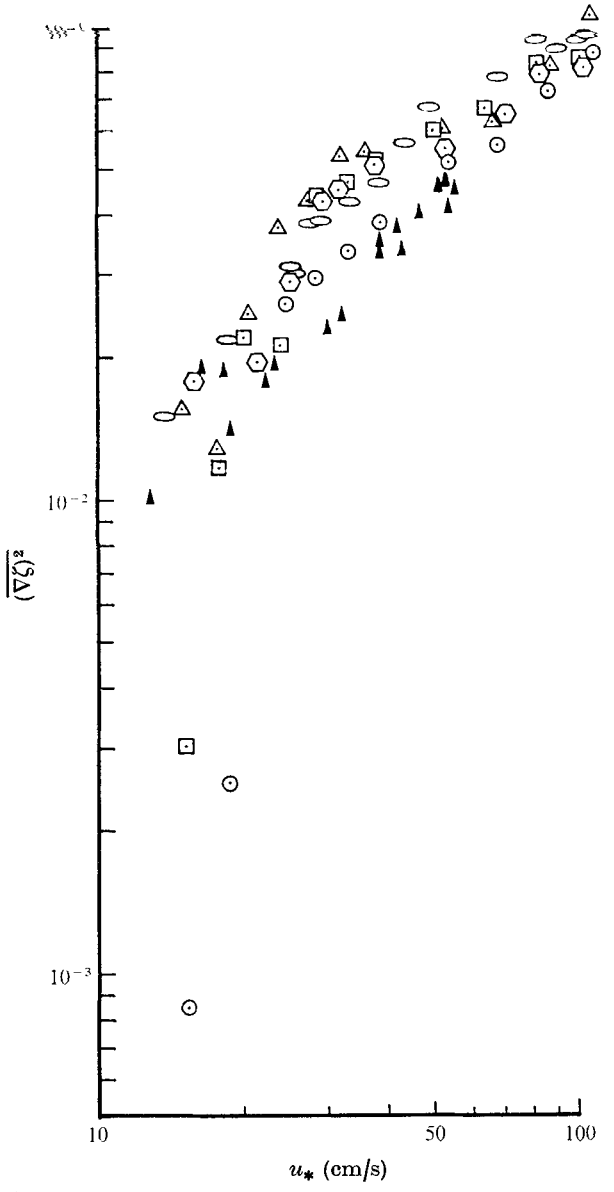

FIGURE 9. $\overline{(\nabla\zeta)^2}$ for the present study in comparison with the Cox (1958) results (▲) and the Wu (1971) results (⬭). Present study: ⊙, fetch = 259 cm; ⊡, ◇, 465 cm; △, 668 cm.

The results indicate that at each wind velocity a quasi-equilibrium state can be established where the spectrum's shape is fixed but its magnitude is still slightly increasing. This seems to indicate that the instability mechanism known as 'cat's paws' as reported by Dorman & Mollo-Christensen (1973) must be important in capillary-wave generation by wind; i.e. most capillary waves in the wind-wave field are probably generated by instability occurring locally at the surface in patches. This occurs even under steady wind conditions. Within

each patch, then, the energy has reached saturated levels and thus the spectrum reaches an equilibrium form. Then, as the wind speed increases, the size or number of patches increases, resulting in an increase in the intensity of the spectrum while it maintains its equilibrium shape. This is a plausible explanation, but one which needs more study.

The combination of a slowly increasing higher frequency component and a change at the peak location probably causes the apparently constant value of $S_{11}^*(1)$ over the 13·5 Hz range.

The overall spectral function compares well with the Cox (1958) result, as shown in figure 8, but the present data display a more orderly variation and relatively low scattering. Since the general shape of the overall envelope follows roughly an n^{-1} curve, the vector sum of the integrated values of $S_{11}(n)$ and $S_{22}(n)$, or $\overline{(\nabla\zeta)^2}$, will change logarithmically with u_*. This result is shown in figure 9 together with the Cox (1958) and Wu (1971) data. These data in figure 9 represent the total mean-square slope $\overline{(\nabla\zeta)^2}$ except for the Wu (1971) result, which is the down-channel or longitudinal component of the mean-square slope. Good agreement is shown throughout the range of measurement.

It is also worth pointing out here that near the peak the spectral shape is different. There is a sharp rise and fall in the spectral values in the immediate neighbourhood of n_0. Although this neighbourhood is precisely the range where all the previous laboratory studies found the existence of an equilibrium range for gravity waves (5 Hz $< n <$ 10 Hz), the present study found no evidence of saturation or an equilibrium state there. The peak region is always much steeper in slope, resembling a hill, as can be easily seen from figure 4, 5 or 8. The shape of the spectrum changes rather abruptly at the end of the 'peak hill', which, presumably, represents the gravity range. The present data seem to suggest that the gravity-wave range has never reached equilibrium under the conditions covered in this study.

The development of the spectra

Limited by our facilities and the data in hand, we can discuss the development of the spectra only for u_* between 15 and 110 cm/s. Up to $u_* = 110$ cm/s all the spectral components are still growing though at a very slow rate. The growth of the spectral components is by no means linear or a monotonic function of wind speed as shown in figure 10. The influence of fetch is again not perceptible. A striking characteristic of the growth is the overshoot as a function of u_*. The growth curves of three frequency components, 5, 13·5 and 56 Hz, are presented in this figure. The contribution of the capillary force to these components is 10 %, 50 %, and 90 % respectively. Each component undergoes rapid growth at $u_* = 15$–20 cm/s. The overshoot occurs at u_* between 20 and 30 cm/s. For a frictional velocity higher than 30 cm/s, the spectral components undergo a gradual increase in magnitude throughout the range of u_*.

The overshoot in the gravity-wave range has been reported by various observers (see, for example, Kitaigorodskii 1970, p. 157) to be a function of fetch. Although only three fetch values were used in the present study, none of the results indicate any fetch influence. An obvious conclusion is that the life

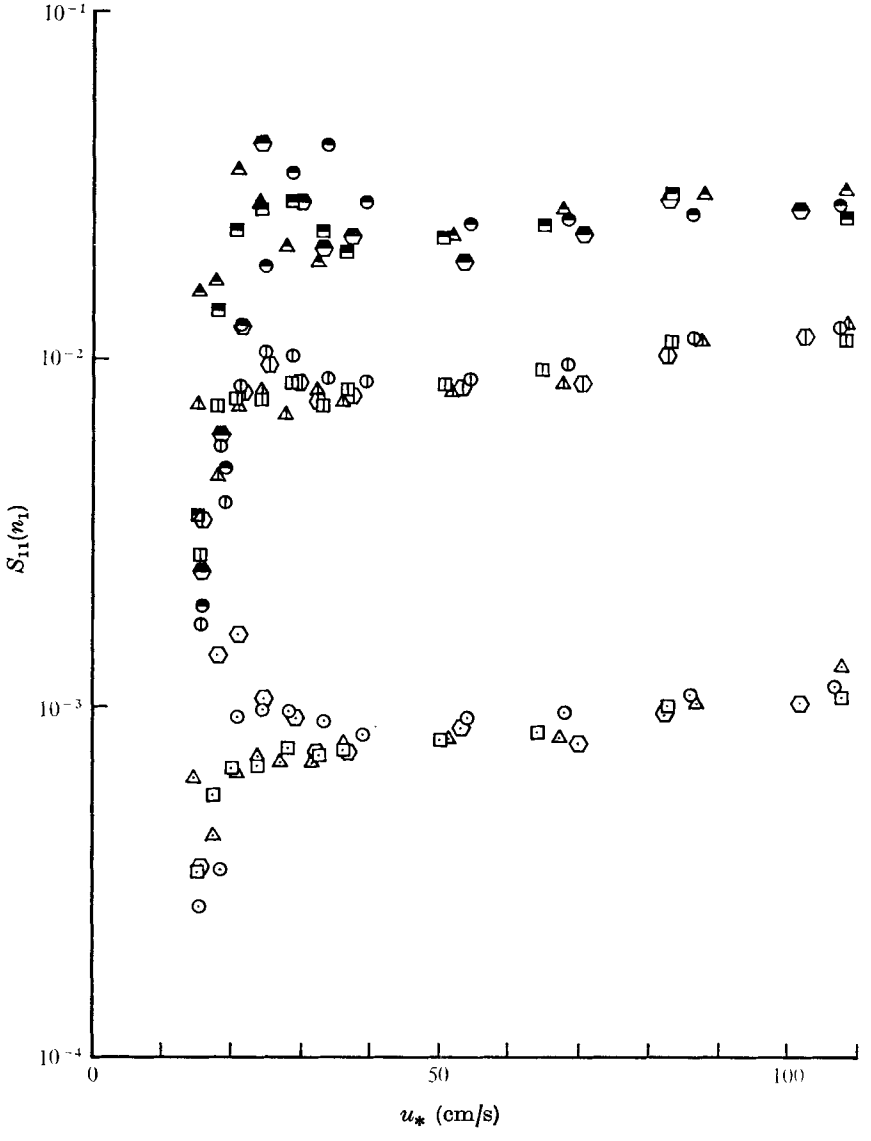

FIGURE 10. The growth of spectral components $S_{11}(n_1)$. Half-filled symbols, $n_1 = 5$ Hz; divided symbols, $n_1 = 13{\cdot}5$ Hz; open symbols, $n_1 = 56$ Hz. Fetches as in figure 9.

span of the higher frequency waves is too short to show any fetch influence at all. But we are not proposing to ignore the fetch in future laboratory studies where controlled conditions of extremely short fetch ($O(1\,\mathrm{m})$) may shed more light on wind-wave generation. Also a rather drastic change occurs around $15\,\mathrm{cm/s} < u_* < 20\,\mathrm{cm/s}$. The dynamic significance of this velocity range can probably be related to the Miles (1962) wind-wave generation study. According to Miles, a minimum frictional velocity of 17·5 cm/s is required to excite waves on a slick-covered water surface. Although all possible precautions were taken to keep the surface clean, it is impossible to keep the surface free of contamination

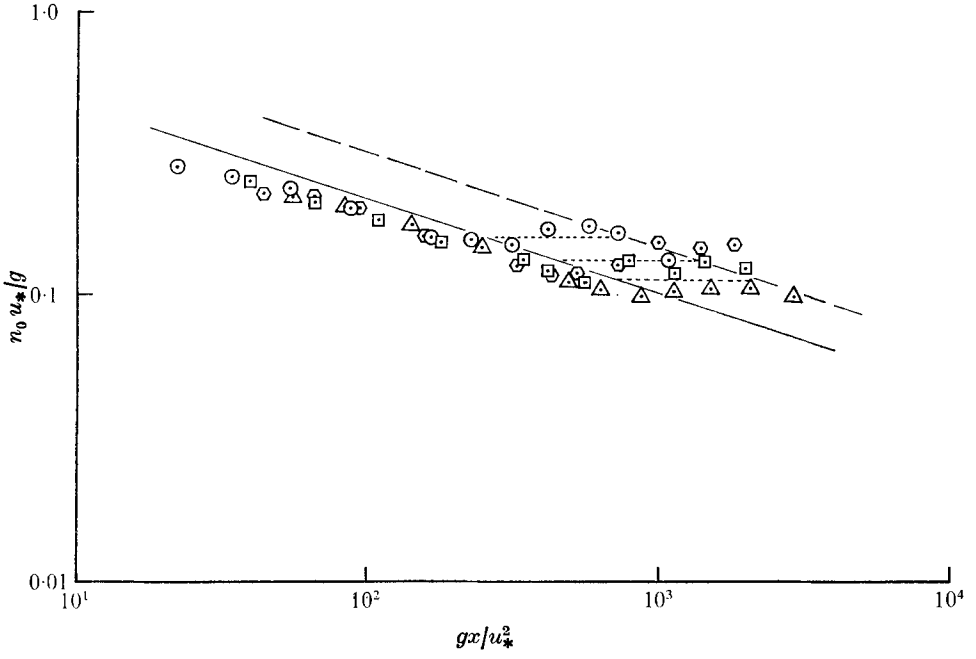

FIGURE 11. $n_0 u_*/g$ as a function of non-dimensional fetch gx/u_x^2.
Fetch: ⊙, 259 cm; ⊡, ⊙, 465 cm; △, 668 cm.

by a film unless continuous skimming is used as indicated by McGoldrick (1970). It is possible that there was some surface film in our tank, since we did not employ continuous surface skimming during the study. If so, the significance of 17·5 cm/s becomes obvious. Unfortunately, we do not have more data at present for $u_* < 15$ cm/s to confirm that waves indeed do not exist for $u_* < 17{\cdot}5$ cm/s.

The development of the spectral peak

From figures 4 and 5 it can easily be seen that the location as well as the magnitude of the spectral peak changes with u_* and the fetch. In previous studies such as Mitsuyasu (1968) and Kitaigorodskii (1970, chap. 7), empirical formulae have been proposed which relate the peak location n_0, the frictional velocity u_* and the fetch X by

$$u_* n_0/g = (u_*^2/gX)^{\frac{1}{3}}. \tag{8}$$

However, in most of the previous studies the u_* values are relatively high and the variation limited, which makes the agreement with (8) impressive but not conclusive. In the present study, a densely varied set of low u_* values was used with three different fetches. The results confirmed (8) only when $u_*^2/g > 1$ cm, i.e. $u_* > 31$ cm/s, as shown in figure 11. When u is less than 31 cm/s, $u_* n_0/g$ assumes a constant value for each fetch, which causes a deviation from the empirical formula (8). Obviously these constant values cannot hold indefinitely as u_* decreases. A limitation on the minimum value of u_* that will be able to generate waves will modify the values eventually. One such candidate is

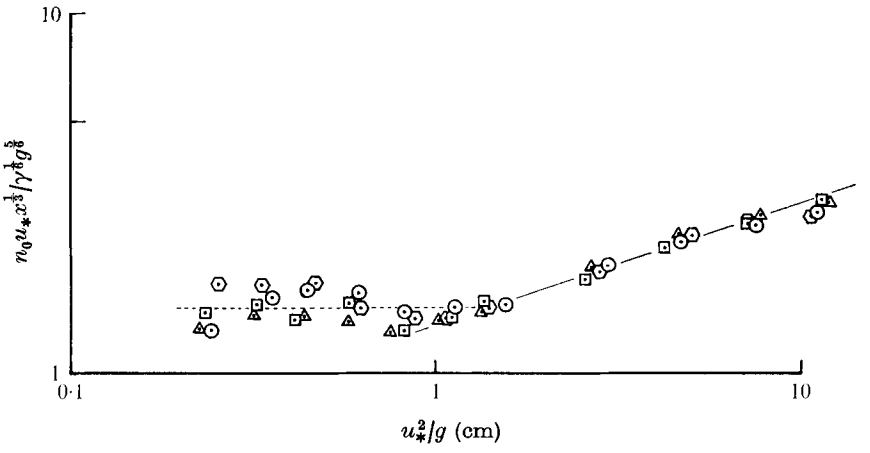

FIGURE 12. $n_0 u_*^{\frac{1}{3}}/g^{\frac{5}{6}}\gamma^{\frac{1}{6}}$ as a function of frictional length scale u_*^2/g from the present study. Symbols as in figure 11.

$u_* = 17{\cdot}5$ cm/s, as discussed in the previous subsection. If this limit is applied, the horizontal dotted line of the constant values should terminate along the dashed line in figure 11. Some of the points are above this limit. It is possible that the slick is not completely packed and that it is only a partially developed slick that is causing the modification. The deviation of the data from the empirical formula indicates that the development of the spectral peak can be divided into two stages by the criterion 1 cm $\gtrless u_*^2/g$, which we define as the frictional length scale. When the frictional length scale is greater than 1 cm, the peak changes follow (8). However, when the frictional length scale is less than 1 cm, $u_* n_0/g$ varies solely with the fetch. The numerical value of the constant for each fetch can be obtained by setting the frictional length scale equal to 1 cm, i.e.

$$\frac{u_* n_0}{g} = \left(\frac{u_*^2}{gx}\right)^{\frac{1}{3}}\Bigg|_{u_*^2/g=1\,\text{cm}.} \tag{9}$$

Under this condition it is likely that the spectral function is controlled not only by the gravity force but also by the capillary force. If so, a new non-dimensional fetch can be defined as gx^2/γ. Keeping the correct power relationship of (9), but employing the new non-dimensional fetch, we get

$$u_* n_0/g \propto (\gamma/gx^2)^{\frac{1}{6}} \quad \text{when} \quad u_*^2/g < 1\,\text{cm}, \tag{10}$$

or

$$u_* n_0 x^{\frac{1}{3}}/g^{\frac{5}{6}}\gamma^{\frac{1}{6}} = \text{constant} \quad \text{when } u_*^2/g < 1\,\text{cm}. \tag{11}$$

When the data in figure 11 are replotted according to (11), the constancy for frictional length scales less than 1 cm becomes obvious; see figure 12. The constant value for 20 points is established as 0·01525 with a standard deviation of 0·001717, or 11·25 %.

The distribution of higher frequency waves on the surface

It is generally accepted that the distribution of higher frequency waves over the surface is not uniform. This conclusion can be derived from theoretical considera-

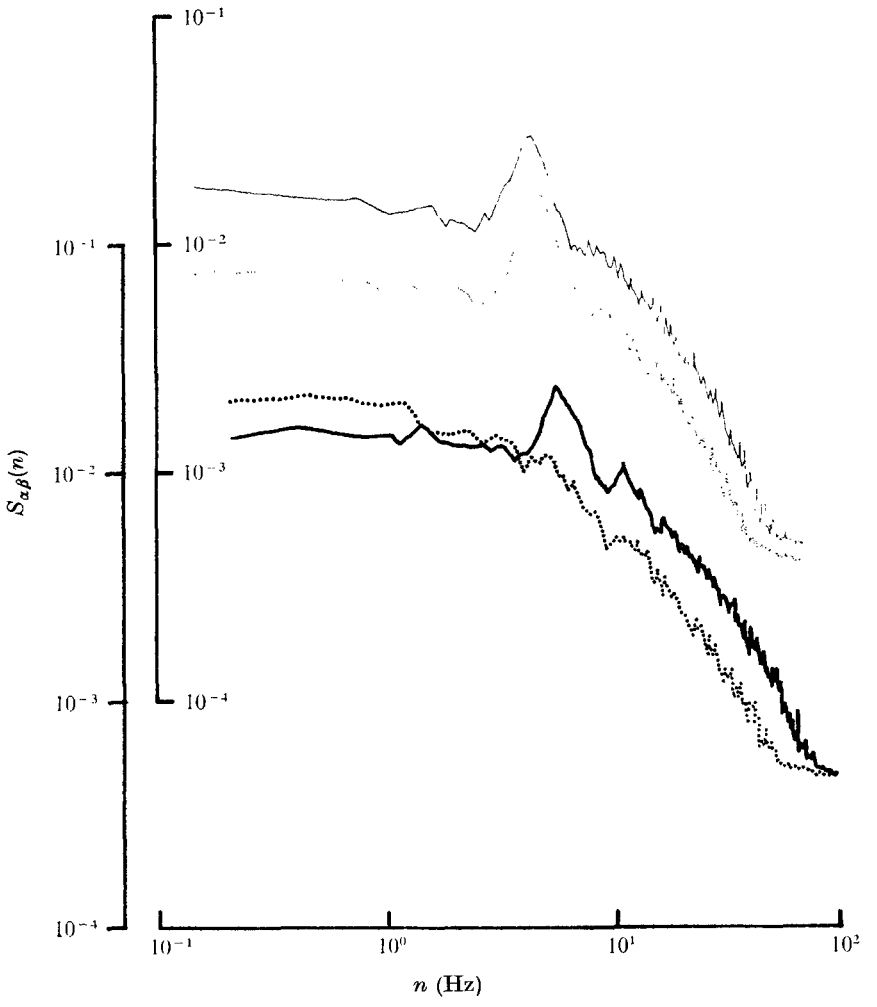

FIGURE 13. Various spectra for $u_* = 35$ cm/s and a fetch of 465 cm. ——, down-channel spectrum S_{11} (upper scale); . . . . ., cross-channel spectrum S_{22} (upper scale); ——, front-slope spectrum (lower scale); . . . . ., back-slope spectrum (lower scale).

tions, but quantitative observational data are not available. In the present study, the diode board has not only been reoriented to obtain down-channel and cross-channel spectra as shown in figure 13, but also has been offset from the zero point for no waves to produce the spectra of front and back slopes as shown also in figure 13. The results indicate that most of the high-frequency waves are on the down-channel, downwind face of the waves. This non-uniform distribution of high-frequency waves can be largely attributed to nonlinear wave–wave interaction and the subsequent parasitic capillary waves as discussed by Crapper (1970).

5. Discussion

Over the years since Phillips (1966) first introduced the equilibrium range for capillary waves, there has existed some level of scepticism among some in the oceanographic community about the existence of a truly equilibrium range primarily because of the lack of data to substantiate the theoretical results. The present study has produced a set of carefully controlled data which strongly support Phillips's concept with some modification. In Phillips's definition as given in (1), the value of n_ν was not clearly defined, even though we use the notion of n_ν. It appears to us that the viscous cut-off frequency is far above the scale considered here. If we start with a common definition of viscous wavenumber as

$$k_\nu = (n/\nu)^{\frac{1}{2}}, \tag{12}$$

with ν = kinematic viscosity, we shall have a rather high value of k_ν. However there are two possible ways to define n_ν. The first is to use the dispersion relation. Since k_ν is a large number, the surface waves will be dominated by surface tension. Then a pure capillary-wave dispersion relation gives

$$n_{\nu 1} = O(\gamma^2/\nu^3) = O(10^9)\,\text{Hz}. \tag{13}$$

This is indeed a very high number. The second approach is to assume that the viscous disturbance is convected by the surface wind drift. Then the frequency is determined by

$$n = u_* k_\nu, \tag{14}$$

under the assumption that the surface drift is directly proportional to the frictional velocity. With this approach, by combining (12) and (14), we get

$$n_{\nu 2} = O(u_*^2/\nu) = O(10^3\text{–}10^5)\,\text{Hz} \tag{15}$$

for the range of wind speed used in this study. In either case, n_ν will be sufficiently separated from n_0 to allow the existence of an equilibrium range.

Finally, it is worthy of note that the spot size of the measuring apparatus must be taken into account, since it has a definite importance in data interpretation. As demonstrated by Sturm & Sorrell (1973), the spot size used can have a drastic effect on the results as the wavelength of the waves observed decreases towards the dimensions of the spot used by the measuring technique. As shown by Sturm & Sorrell (1973), an error of approximately 10% by a capacitance probe was indicated when compared with a laser device as the wavelength decreased to roughly ten times the spot size of the capacitance probe, represented by its meniscus diameter of approximately 6 mm. The comparison was made for monochromatic waves, so that the slope signal of the laser device could be processed electronically to yield the wave height. When the laser-beam diameter of 0·33 mm used in the comparison is expanded to approximately the size of the meniscus of the capacitance probe (6 mm), then good agreement is observed between the capacitance probe and the laser device, as shown also in the work of Sturm & Sorrell (1973). This indicates then, that any device used to obtain a real time record of wave amplitude or slope is wavelength or frequency limited. This limit is approached as the wavelengths measured decrease to values roughly equal to or less than ten times the spot size.

The present study used a spot size of 0·5 mm, indicating an ability to measure wave parameters accurately for waves down to a wavelength of 5 mm, corresponding to a frequency of approximately 63 Hz. Beyond 63 Hz, the error due to spot size is approximately 10 % and increases with increasing frequency. In the study of Cox (1958), a spot size of 0·7 mm was used for the frequency spectra of slope, indicating a wavelength limit of 7 mm, or approximately 39 Hz. For the mean-square slope measurements of Cox (1958), a 2 mm spot size was used, implying a limit of 2 cm in wavelength, or about 12 Hz. Thus the 2 mm spot size tended to filter out or reduce any contributions to the mean-square slope from waves of frequency greater than about 12 Hz. This could account in part for the results of the present study being greater than the Cox (1958) mean-square slope values. Wu (1971) gave an acceptance width of 1° for the instrument used, but no spot size was given.

The authors wish to express their appreciation for the help and assistance provided by Dr F. Y. Sorrell and Mr Andrew Withers during the experimental phase of the study. Gratitude is also expressed by SRL for the support provided by Contract NAS6-2617 from the NASA Wallops Flight Center, for the support provided by the Center for Marine and Coastal Studies, North Carolina State University, and for the co-operation and help of the Department of Geosciences, North Carolina State University.

REFERENCES

BANNER, M. L. & PHILLIPS, O. M. 1974 On the incipient breaking of small scale waves. *J. Fluid Mech.* **65**, 647–656.

COX, C. S. 1958 Measurements of slopes of high frequency wind waves. *J. Mar. Res.* **16**, 199–225.

COX, C. S. & MUNK, W. H. 1956 Measurements of the roughness of the sea surface from photographs of the sun's glitter. *Bull. Scripps Inst. Ocean., Univ. Calif.* **6**, no. 9.

CRAPPER, G. D. 1970 Non-linear capillary waves generated by steep gravity waves. *J. Fluid Mech.* **40**, 149–159.

DORMAN, C. E. & MOLLO-CHRISTENSEN, E. 1973 Observation of the structure of moving gust patterns over a water surface ('cat's paws'). *J. Phys. Ocean.* **3**, 120–132.

HUANG, N. E., SORRELL, F. Y., TUNG, C. C., GUTMAN, N., LONG, S. R. & STURM, G. V. 1974 Ocean dynamics studies – of current–wave interactions. *N.A.S.A. Contractor Rep.* no. CR-137467.

JONES, W. L., GRANTHAM, W. L., SCHROEDER, L. C., JOHNSON, J. W., SWIFT, C. T. & MITCHELL, J. L. 1975 Microwave scattering from the ocean surface. *I.E.E.E. Trans. Microwave Theor. Tech.* 1053–1058.

KITAIGORODSKII, S. A. 1970 *The Physics of Air–Sea Interaction.* Jerusalem: Keter Press.

LARSON, T. R. & WRIGHT, J. W. 1975 Wind-generated gravity–capillary waves: laboratory measurements of temporal growth rates using microwave backscatter. *J. Fluid Mech.* **70**, 417–436.

MCGOLDRICK, L. F. 1970 An experiment on second-order capillary gravity resonant wave interactions. *J. Fluid Mech.* **40**, 251–271.

MILES, J. W. 1957 On the generation of surface waves by shear flows. *J. Fluid Mech.* **3**, 185–204.

MILES, J. W. 1962 On the generation of surface waves by shear flows. Part 4. *J. Fluid Mech.* **13**, 433–448.

MITSUYASU, H. 1968 On the growth of the spectrum of wind generated waves. I. *Rep. Res. Inst. Appl. Mech., Kyushu Univ.* **16**, 459–482.

PHILLIPS, O. M. 1957 On the generation of waves by turbulent wind. *J. Fluid Mech.* **2**, 417–445.

PHILLIPS, O. M. 1958 The equilibrium range in the spectrum of wind-generated waves. *J. Fluid Mech.* **4**, 426–434.

PHILLIPS, O. M. 1966 *The Dynamics of the Upper Ocean.* Cambridge University Press.

PHILLIPS, O. M. & BANNER, M. L. 1974 Wave breaking in the presence of wind drift and swell. *J. Fluid Mech.* **66**, 625–640.

STURM, G. V. 1973 Experimental studies of capillary waves on currents. Ph.D. thesis, Department of Engineering Mechanics, North Carolina State University at Raleigh. University Microfilms, Ann Arbor, Michigan.

STURM, G. V. & SORRELL, F. Y. 1973 Optical wave measurement technique and experimental comparison with wave height probes. *Appl. Opt.* **12**, 1928–1933.

WU, J. 1968 Laboratory studies of wind–wave interactions. *J. Fluid Mech.* **34**, 91–111.

WU, J. 1971 Slope and curvature distributions of wind-disturbed water surface. *J. Opt. Soc. Am.* **61**, 852–858.